Available online at www.sciencedirect.com
SCIENCE DIRECT
Sensors and Actuators A 123–124 (2005) 540–546
SENSORS AND ACTUATORS A PHYSICAL
www.elsevier.com/locate/sna

# Simulation of shaped comb drive as a stepped actuator for microtweezers application

Isabelle P.F. Harouche, C. Shafai *

*Department of Electrical and Computer Engineering, University of Manitoba, Winnipeg, Man., Canada R3T 5V6*

Received 4 September 2004; received in revised form 13 March 2005; accepted 25 March 2005
Available online 22 April 2005

**Abstract**

Finite element analysis is used to simulate electrostatic actuated, shaped comb drives operating under dc conditions (zero actuating frequency). A dynamic multiphysics model is developed using the arbitrary Lagrangian–Eulerian (ALE) formulation. Results show the coupled interaction between the electrostatic and mechanical domains of the transducer. The analysis is based on the evolution of electrostatic force versus comb finger engagement. The relationship between incremental lateral displacement and actuation voltage illustrates the potential for stepped movement for a shaped comb drive. Additionally, through numerical simulations, this project determines an optimum design for a dc-actuated comb drive, which has controllable force output and stable engaging movement.


*Keywords:* Microtweezers; MEMS; Comb drive; FEM; ALE

## 1. Introduction

Capacitance-based sensors and actuators have been extensively used in micro electromechanical systems (MEMS) devices [1,2]. Among different devices, the most commonly used and analysed is the comb drive [3,4]. The MEMS comb drive is a laterally driven mechanical actuator activated by electrostatic interaction. The basic design of a comb drive relies on the theory of parallel-plate capacitors, which in turn is a function of the plates' area and shape. In the case of a comb drive, the parallel plates are an array of interdigitated fingers, which are generally rectangular. A typical rectangular-shaped comb drive design requires simple fabrication steps (usually only one structural layer) and it is characterized by low power consumption [5]. The device has a constant force-to-displacement relationship, which is a function of the change in capacitance with respect to engagement, rather than total capacitance. Rectangular comb drives have been used as actuators for several different applications, including micro-motors, conveyors, sensing devices and microgripper devices.

Later, shaped comb drives were introduced as a means to tailor the rate of change of capacitance with respect to the lateral displacement. Designs presented in literatures [6,7] were used to stiffen and weaken resonator springs and hence offer more controllability over the device operation. These tunable *resonators* were introduced as a means to achieve more linear force-engagement profiles.

The present work discusses a novel move-and-lock mechanism based on a shaped comb drive design. The main use for such device is as a microtweezers actuator for application in areas such as biological sample handling, MEMS assembly processes and other activities where precision micromanipulation and force-controlled interaction are required.

## 2. Design concept

This project introduces an adaptation to the parabolic-shaped comb drive analysed in [6], in that the force–displacement is not linear, but it is also not constant, as in the case of rectangular comb drives. Instead, a

* Corresponding author. Tel.: +1 204 474 6302; fax: +1 204 261 4639.
*E-mail addresses:* harouche@ieee.org (I.P.F. Harouche), cshafai@ee.umanitoba.ca (C. Shafai).

0924-4247/$ – see front matter © 2005 Elsevier B.V. All rights reserved.
doi:10.1016/j.sna.2005.03.031

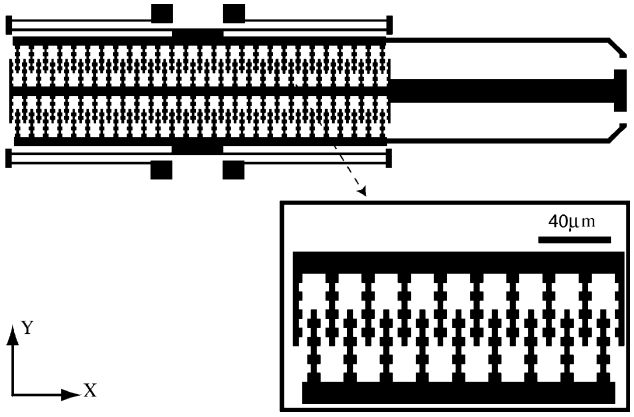


Fig. 1. Illustration of the design for the shaped comb drive as a microtweezers actuator. The blow-up image shows a representation of a jagged-edge comb drive.

stepwise continuous response of force versus displacement occurs. Fig. 1 offers a conceptual idea of a possible final design for the force controllable microtweezers, whereas the insert depicts a section of the comb drive itself. The proposed move-and-lock mechanism is based on the change in the distance between the comb fingers with respect to engagement, which in turn is a function of the actuation voltage.

The geometry simulated corresponded to a set of 10 fixed fingers and 9 movable fingers. Fig. 2 presents all geometries analysed throughout this paper and should be used as a reference. The designs had a few dimensions in common, namely the length of each finger, which was 40 μm long with notches at 5 μm intervals, and the structural thickness of 2 μm. The set of movable fingers start at a rest position corresponding to a 20 μm engagement. The design of Fig. 2A has minimum and maximum gap distances between fingers of 3 and 7 μm, respectively. This design complies with the requirements for the Multi-User *MEMS* Process (MUMPs) [8]. This report, however, attains to the actuator design. The gripping pads and final microtweezers testing are left for future work.

## 3. Electromechanical principles of the comb drive

The comb drive is a capacitive device with air as the dielectric material. The region where the problem is defined is charge free ($\rho_V = 0$) and the electrostatic problem is described by Laplace's equation (in rectangular coordinates):

$$\nabla^2 V = \frac{\partial^2 V}{\partial X^2} + \frac{\partial^2 V}{\partial Y^2} + \frac{\partial^2 V}{\partial Z^2} = 0 \tag{1}$$

Finite element simulations were carried out to find potential distributions which satisfy Eq. (4) for a given electrode geometry at a predefined actuation potential $V_0$. Since there was no current flow inside the comb drive device itself, the surface of the device was assumed equipotential. Potential energy was a continuous quantity in the domain of interest; hence, the fundamental requirement of the finite element method was met. The voltage-dependant continuous field can be approximated by a discrete model composed of a set of piecewise continuous functions defined over a finite number of subdomains.

Once the scalar field $V$ is know, electric energy $W_e$ is computed at all elements according to

$$W_e = \frac{1}{2}\varepsilon_0 \iiint_{XYZ} |\boldsymbol{E}|^2 \, dX \, dY \, dZ \tag{2}$$

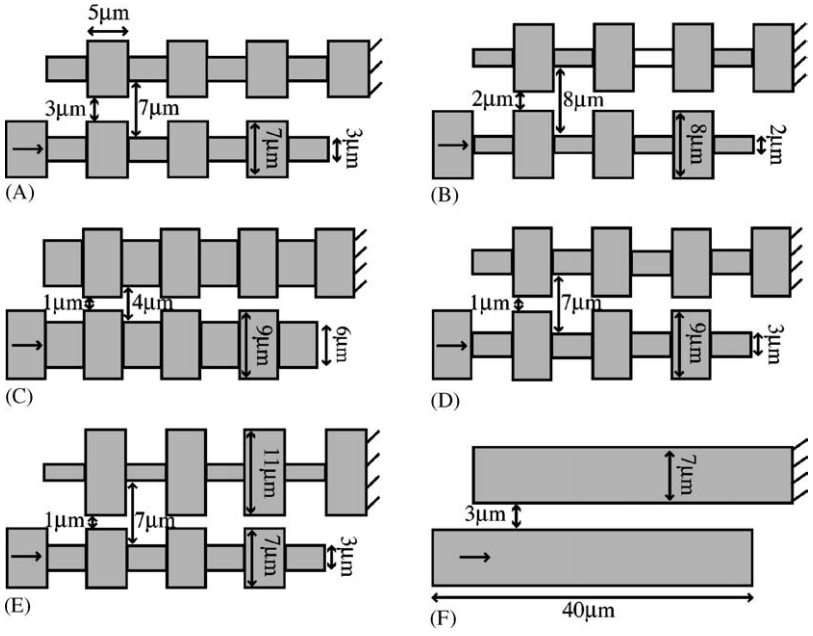


Fig. 2. The five jagged-edge comb designs analysed. Design "A" complies with the MUMPs standard dimensions.

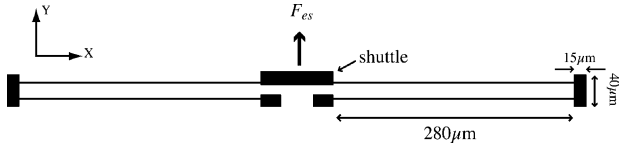


Fig. 3. Schematic description of the simulated spring; $F_{es}$ denotes the load force, which corresponds to the electrostatic force generated by the comb drive. The shuttle is the mounting structure where the comb drive is attached.

Computations for capacitance $C$ and electrostatic force $F_{es}$ follows, as shown in Eqs. (3) and (4). The solution of the electrostatic problem served as the load to the mechanical problem:

$$C_{TOT} = \frac{2}{V_0^2} \iiint_{XYZ} W_e \, dX \, dY \, dZ \tag{3}$$

$$F_{es} = \frac{\partial W_e}{\partial Y} = \frac{1}{2} \frac{\partial C}{\partial Y} V_0^2 \tag{4}$$

The reader is encouraged to find detailed description of the electrophysics of comb drives elsewhere 0.

### 3.1. Mechanical characterization of the comb drive

The design of the springs followed the specifications in Fig. 3. The movable set of fingers is attached to a shuttle, which in turn is the link between the electrostatic force-generating device and the two double-folded cantilever beam springs. Hence, the comb displacement was a combination of electrostatic pulling force $F_{es}$ and the mechanical spring restoring force $F_{mech}$:

$$F_{mech} = k\Delta Y \tag{5}$$

The following definitions applied to the cantilever springs: (a) the material used in the fabrication (polysilicon) was assumed homogeneous and isotropic; (b) the thickness dimension was small compared to the length; and (c) the stress in the normal $Z$-direction was ideally zero. It is nevertheless worth noting that in non-ideal testing environment the levitation phenomena contributes to a finite $Z$-component of stress. In any case, levitation analysis was beyond the scope of this paper. The stresses and loads were defined in the $X$–$Y$ plane and so any other parallel plane has the same stress distribution. Thus, the springs fell into the characteristic plane stress problem definition [10].

## 4. Numerical analysis

Proper dynamic analysis of the device required coupled electromechanical analysis. Simulations were performed in the 2D domain using the finite element method (FEM) in the FEMLAB 3.0a software package [11]. Meshes were automatically generated by the software. Given the comparative nature of this work, where each simulation run must be analysed with respect to each other, a mesh analysis was performed prior to simulations. The goal was to achieve a mesh density that could be reasonably matched amongst all runs. Electrostatic simulations were performed for several different mesh densities for linear and quadratic elements. The densities chosen followed the standard options available in FEMLAB 3.0a varying from extremely coarse to extremely fine densities. Fig. 4 shows that quadratic elements returned similar results irrespective of mesh density. As for the linear elements, the range of results varied up to 14%. Based on these results, all simulations were computed from quadratic elements using FEMLAB's automatically generated coarser mesh.

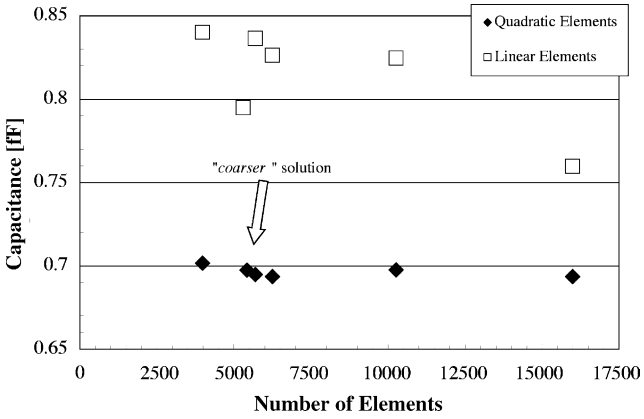


Fig. 4. Mesh density analysis. The arrow points to the FEMLAB 3.0a standard "coarser" mesh solution. For this analysis, the coarser mesh returned approximately 5000 elements.

Basic comb drive theory indicates that fringing fields in the third dimension are of some importance in the computation of electrostatic force [9]. However, due to processing time and memory requirements, simulations were performed in a 2D environment. That excluded field lines in the third dimension. In any event, discrepancies between 2D- and 3D-capacitance analysis were investigated as a means to bring model results into the context of actual fabricated devices. Fig. 5 presents the results of a simple model of two parallel rectangular plates

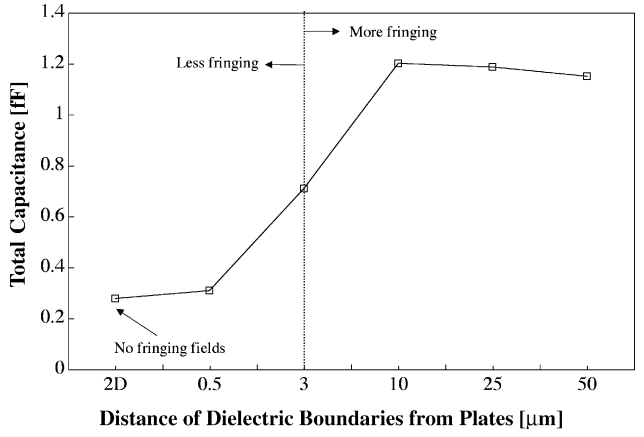


Fig. 5. Comparison between 2D and 3D capacitance computations. The $x$-coordinates depict the distance between the device boundaries and the surrounding volume boundaries.

with the same dimensions as the analysed comb fingers. The plates were kept at a constant 3 μm distance from each other. The distance to the surrounding dielectric volume boundary was varied. Note that the volume of integration directly affects the amount of fringing fields accounted for in the final scalar values. The plot in Fig. 5 shows that the total capacitance of the 3D system is approximately four times that of the 2D system. Since the direct relationship between input voltage and capacitance is expressed as $C = 2W_e/V_0^2$, a quick dimensional examination tells us that the required input voltage for 2D simulations should be twice as large as the 3D case.

### 4.1. The arbitrary Lagrangian–Eulerian formulation

The generation of successful multiphysics models was not trivial, due to the complexity of the geometry and the large deformations at the spring. Difficulties arose in developing a mesh capable of approximating large deformations. Additionally, a dynamic parametric simulation was bound to generate increasingly deformed meshes, which in turn became unstable and solutions did not converge. The arbitrary Lagrangian–Eulerian (ALE) technique is an advanced method of solving moving boundaries and non-linear problems in finite element analysis (FEA) [12–14]. The ALE method was chosen as a means to avoid such lack of convergence. Additionally, ALE can be used as a powerful tool for multiphysics analysis, a common trait in MEMS design. It has not yet been widely explored in MEMS transducer simulation. Upon extensive investigation, only one other research paper was found on MEMS simulation using ALE [15].

Basic ALE formulations are available from different sources [12,16,17], which can be used as an initial template and adapted to each specific problem. The basis of the technique is to use an FE mesh that is neither attached to the material nor fixed in space. An arbitrary motion independent of the material deformation is assigned to each degree of freedom of the system. The main advantage of this technique lays in the fact that at any point of the analysis a solution may be computed. Both in cases where large and highly localized deformation of the structure occur, and where unconstrained flow of material on free boundaries happens.

One characteristic of the ALE formulation is that the solution variables representing structural deformation are only determined at elements within the structure boundaries. The coupling with other simulation variables happens through the mesh displacement characteristics. Thus the structure deformation properties must be transferred to mesh points through an updating algorithm. Additionally, prescribed mesh displacements must be assigned for all degrees of freedom of the mesh, at each iteration of the numerical solution [18]. The algorithm performs an automatic grid re-design procedure, which maps the original domain into the deformed domain at each displacement instance. Hence, the ALE formulation specifies which boundaries will move during the simulation and how they should move.

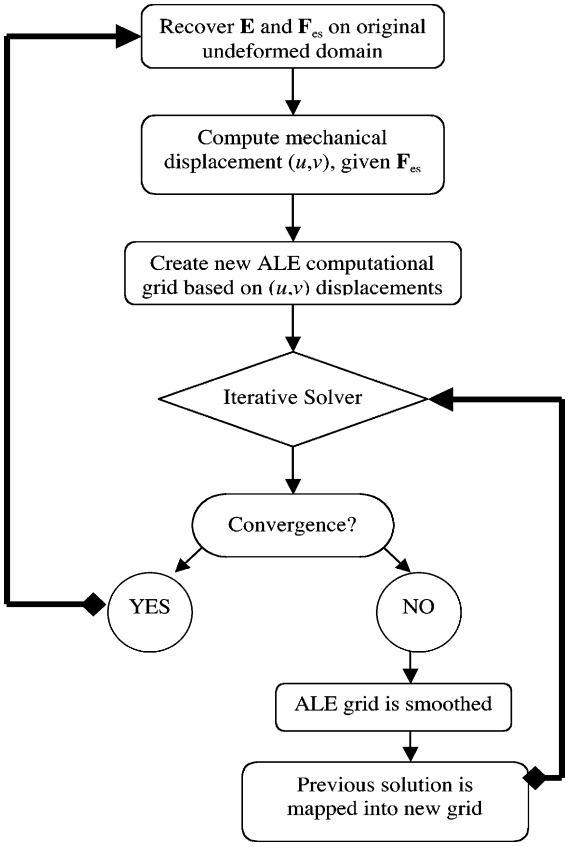


Fig. 6. Flowchart describing the ALE procedure.

For the purpose of this research, the ALE formulation was used to solve the electrostatic problem defined in the dielectric domain. Both electrostatic and mechanical simulations were performed concurrently and the solution of the former served as a boundary condition to the latter. Thus, the ALE formulations can be described as an algorithm that performs automatic reasoning [19], as seen in the flow chart in Fig. 6.

The ALE mesh displacements were defined by Poisson's equation and solved in integral form, as seen in the following equations:

$$\int_\Omega \det \mathbf{J}[(\hat{\delta}x_X I_{Xx} + \hat{\delta}x_Y I_{Yx})\delta x_x + (\hat{\delta}x_X I_{Xy} + \hat{\delta}x_Y I_{Yy})\delta x_y]\,\mathrm{d}\Omega = 0 \quad (6a)$$

$$\int_\Omega \det \mathbf{J}[(\hat{\delta}y_X I_{Xx} + \hat{\delta}y_Y I_{Yx})\delta y_x + (\hat{\delta}y_X I_{Xy} + \hat{\delta}y_Y I_{Yy})\delta y_y]\,\mathrm{d}\Omega = 0 \quad (6b)$$

where (6a) and (6b) represent the $x$- and $y$-components in the computational ALE mesh domain and the hat symbol defines a test function. The term ($\det \mathbf{J}$) is the determinant of the inverse Jacobian which maps the original coordinates in ($X$,$Y$) to the deformed coordinates ($x$,$y$). It follows that $u = x - \mathrm{X}$ and $v = y - \mathrm{Y}$. The electrostatic equation starts with Gauss' law,

presented in integral forming the following equation:

$$\varepsilon \int_{\Omega} \det \mathbf{J}[(\hat{V}_X I_{Xx} + \hat{V}_Y I_{Yx})V_x + (\hat{V}_X I_{Xy} + \hat{V}_Y I_{Yy})V_y]\,\mathrm{d}\Omega = 0 \quad (7)$$

where $I_{ij}$ corresponds to the entries in the inverse Jacobian matrix.

The mechanical variables of interest were the global spring displacements $(u, v)$ in the $X$- and $Y$-directions. The solution for the spring problem was derived from the PDE form of Navier's equations for the $X$- and $Y$-components (Eq. (8)), where $c$ is a coefficient dependent on the Young's modulus $E$, the Poisson's ratio $\nu$, $\rho$ is the density of the material. Additionally $\mathbf{u} = (u, v)$ is the displacement vector:

$$\rho \frac{\partial^2 \mathbf{u}}{\partial t^2} - \nabla \cdot c\nabla \mathbf{u} = \mathbf{K} \quad (8)$$

The vector $\mathbf{K}$ represents the force applied to the shuttle, which in turn is connected to the springs and therefore acts as the load in this system. Hence $\mathbf{K}$ is the derived from the electrostatic force computed in the ALE part of the simulation. Both mechanical and electrostatic solutions combined gave the desired comb drive dynamic characterization.

## 5. Results and discussion

Parametric computations returned the field distribution in the dielectric for input potentials from 0 to 250 V. Forces acting upon the set of movable fingers were computed at each increment of voltage. Fig. 7a shows a plot of the electrostatic force acting on the comb teeth of design A (shown in Fig. 2), as a function of the finger displacement due to the applied voltage. It can be seen that the response is similar to that expected from a rectangular-shaped comb drive. This is corroborated by the plot in Fig. 7b, which shows the electrostatic force behaviour for a rectangular comb drive with the same length, thickness, and minimum gap as the jagged-edge structure. The difference between these two results is very noticeable when observed in terms of the force gradient, shown in the secondary axes of Fig. 7. The jagged-edge shaped of design A produces an evident variable rate of change in force with respect to engagement. The absolute values of the force gradient are however too small for this design to possess stepped displacement.

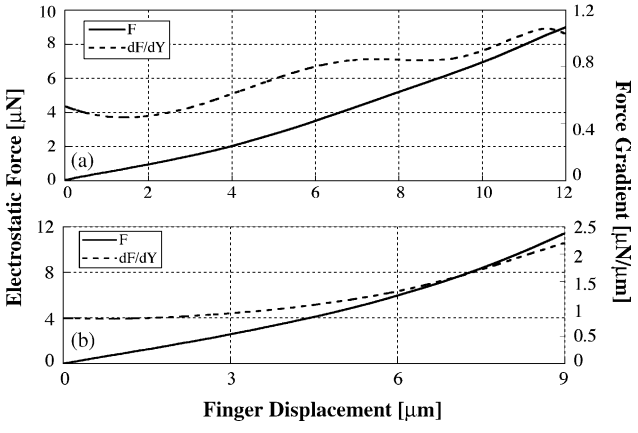


Fig. 7. Plots of force and force gradient with respect to finger engagement from rest position. Engagement distance was computed from the incremental application of voltages from 0 to 250 V: (a) the forces acting on the jagged-edge fingers of design A; (b) the forces acting on a set rectangular fingers of similar dimensions.

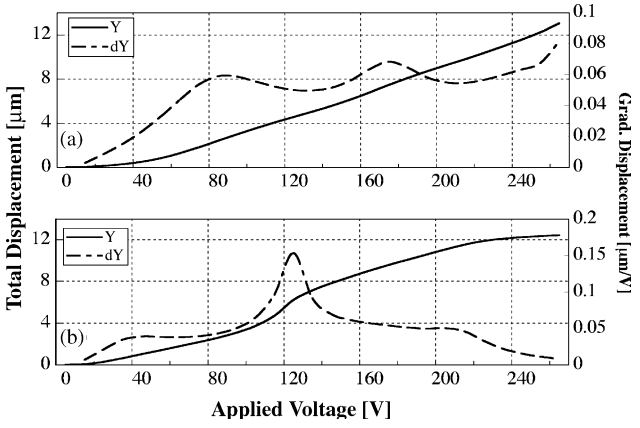


Fig. 8. Comb displacement with respect to $V_0$: (a) results from the 8:2 μm gap; (b) results from the 4:1 μm gap. The reader should note the difference in scales in the differential displacement axes.

Next, designs B and C of Fig. 2 where investigated. These two designs both have a 4:1 relationship between maximum and minimum gap size, but with different dimensions. The FEM simulation results (Fig. 8a) show that design B's 8:2 μm gap results in two points of inflection, which are more noticeable than the result for the geometry of design A, but still the absolute displacement values are not enough to justify the design. Design C's 4:1 μm gap spacing (Fig. 8b) renders an evident step in the total displacement, but the expected "locking positions" shows some minute slippage. This can be seen as the plateaus in the curve for differential displacement with respect to input voltage. The ideal locking position would have zero displacement gradient with respect to the actuation voltage. In Fig. 9, it can be seen that the force gradient for design C shows a change of inflection at 4 μm displacement from rest position and break points at 6 and 11 μm displacement. These results show that the total electrostatic force acting upon the movable fingers is seven times larger than those observed in the 8:2 μm gap design.

From the above results it is evident that the key factor in the jagged-edge shape design is the ratio between maximum and minimum gaps in conjunction with the actual minimum gap distance value. From the results, the 4:1 ratio with 1 μm minimum gap is more effective than the 4:1 with 2 μm minimum gap. Thus, we deduce that, for increased gap distances, the dimension of each notch must be increased as well. That is so the gain in notch area balances the increase in gap distance, preserving the total electric energy, as seen in the following

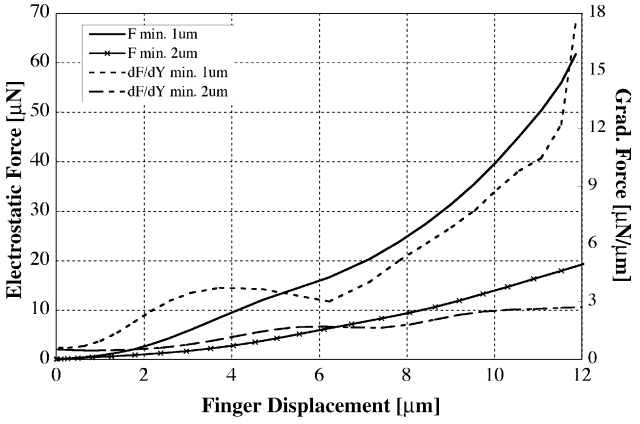


Fig. 9. Force and force gradient results for both 4:1 μm gap and 8:2 μm gap designs. The values for the 4:1 μm gap design is seven times larger than those seen in Fig. 7.

equation:

$$W_e = \frac{1}{2}\frac{\varepsilon A}{d^2}V_0^2 \tag{9}$$

Designs D and E of Fig. 2 have exaggerated ratios between minimum and maximum distances with respective values of 1 and 7 μm gaps. Design E, however, is constructed in such a way that the gaps are asymmetric with respect to the imaginary line between the two fingers.

Results for this last analysis are shown in the context of all previous simulations. Fig. 10 shows combined plots of displacement gradient with respect to actuation voltage. Note that the asymmetric 7:1 design shows two clear points of inflection. The first step in displacement occurs at about 40 V. By observing the slope of the curve, it is possible to infer an increase in velocity, which implies that the movable comb finger accelerates. It then decelerates to a constant, stable and small displacement. Ideally, the structure should almost lock in place preventing any *Y*-direction movement. When the input potential reaches 150 V another surge in acceleration happens. At this point, the total amount of displacement is larger than in the previous engagement. The general behaviour of the 7:1 symmetric design was similar, but the points of inflection are not as accentuated and the trough not as low, implying more slippage.

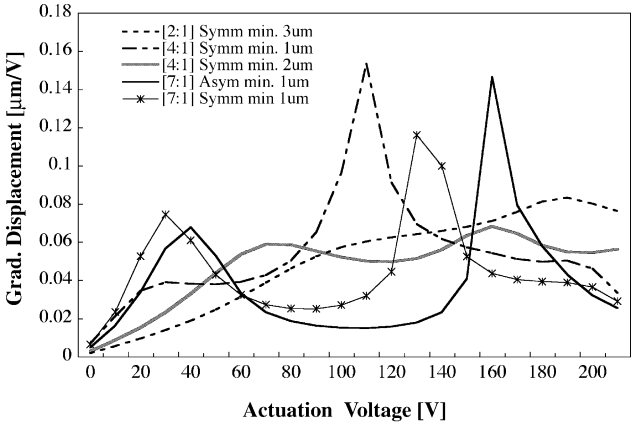


Fig. 10. Comparison of differential displacements of all geometries investigated.

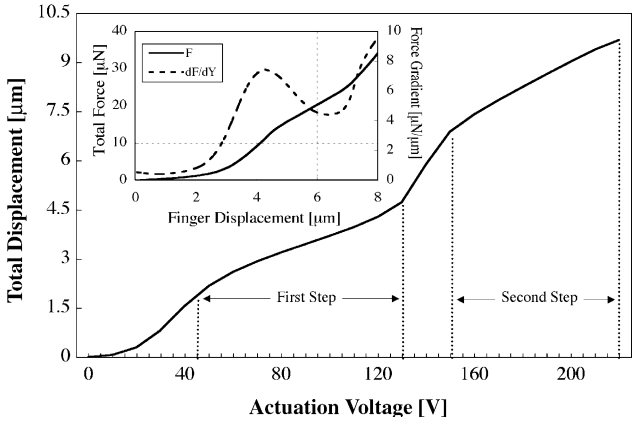


Fig. 11. Analysis of the 7:1 symmetric design (shape "D").

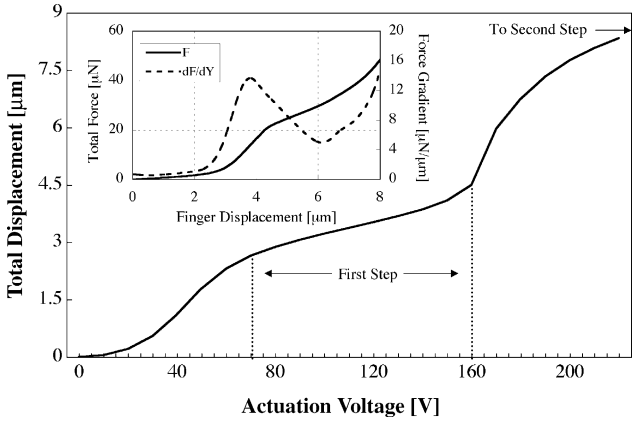


Fig. 12. Analysis of the 7:1 asymmetric design (shape "E").

Figs. 11 and 12 illustrate the 7:1 designs in detail. The symmetric design (Fig. 11) has two engagement steps, but the slippage in the asymmetric design (Fig. 12) is smaller. It follows that the point of inflection in the force versus displacement plot is more evident in the asymmetric case.

These results illustrate the concept of step movement and show that, for a given gap ratio, there exists an optimum design correspondent to an asymmetric geometry. Notable points of improvement in the design are: (1) optimization of the jagged notch length with respect to structural thickness, which balances the influence of gap distance, and (2) consideration of the slippage problem, which prevents total locking of the device.

## 6. Conclusions

This paper has introduced a novel application to MEMS comb drives operating under dc conditions. The jagged-edge shaped finger was simulated using finite element analysis

and applying the arbitrary Lagrangian–Eulerian formulation. Initial results based on the MUMPs standard dimensions were not conclusive; consequently, new dimensions were tested. Upon simulating different jagged-edge designs, it has been found that the key to achieving the proposed move-and-lock mechanism is optimization of the maximum to minimum gap relationship. Based on the designs investigated, the optimum result came from an asymmetric 7:1 gap ratio, for a device with 2 μm thick structural layer. Further work is required to define an analytical model for the jagged-edge comb drive. However, at this point numerical solutions were adequate to prove the concept of stepped-movement.

## Acknowledgements

This research has been funded by the Health Science Centre Foundation, Winnipeg, MB, and the Natural Sciences and Engineering Research Council (NSERC) of Canada. The authors wish to thank Mr. Behraad Bahreyni (Electrical and Computer Engineering, University of Manitoba) and Mr. Linus Andersson (Comsol, AB) for their suggestions during the course of this work.

## References

[1] C. Lu, M.A. Lemkin, B.E. Boser, A monolithic surface micromachined accelerometer with digital output, IEEE J. Solid-State Circuits 30 (1995) 1367–1373.
[2] E.J. Garcia, J.J. Sniegowski, Surface micromachined microengine as the driver for micromechanical gears, in: Proceedings of the International Conference on Solid-State Sensors and Actuators, Stockholm, Sweden, 1995, pp. 365–368.
[3] W.C. Tang, T.-C.H. Nguyen, R.T. Howe, Laterally driven polysilicon resonant microstructures, in: Proceedings of the Technical Digest IEEE Micro Electro Mechanical Systems Workshop, Salt Lake City, UT, 1989, pp. 53–59.
[4] W.C. Tang, Electrostatic comb drive for resonant sensor and actuator application, Ph.D. Dissertation, University of California, Berkeley, CA, 1990.
[5] G.T.A. Kovacs, Micromachined Transducers Sourcebook, McGraw-Hill, 1998.
[6] B.J. Jensen, S. Mutlu, S. Miller, K. Kurubayashi, J.J. Allen, Shaped comb fingers for tailored electromechanical restoring force, J. Microelectromech. Syst. 12 (3) (2003) 373–383.
[7] W. Ye, S. Mukherjee, N.C. MacDonald, Optimal shape design of an electrostatic comb drive in microelectromechanical systems, J. Microelectromech. Syst. 7 (1) (1998) 16–26.
[8] D.A. Koester, R. Mahadevan, B. Hardy, K.W. Markus, MUMPs Design Handbook, Revision 7.0, Cronos Integrated Microsystems, Research Triangle Park, NC, USA, 2001.
[9] W.A. Johnson, L.K. Warne, Electrophysics of mechanical comb actuators, J. Microelectromech. Syst. 4 (1) (1995) 49–59.
[10] V. Adams, A. Askenazi, Building Better Products with Finite Element Analysis, Onword Press, Santa Fe, NM, USA, 1999.
[11] Femlab Reference Manual, Comsol, AB, 2003. http://www.comsol.com.
[12] J.-P. Ponthot, Advances in arbitrary Eulerian–Lagrangian finite element simulation of large deformation processes, in: Proceedings of the Fourth International Conference on Computational Plasticity (COMPLAS IV), Barcelona, Spain, 1995, pp. 2361–2372.
[13] J. Wang, M.S. Gadala, Formulation and survey of ALE method in nonlinear solid mechanics, Finite Elem. Anal. Des. 24 (1997) 253–269.
[14] P. Vachal, R.V. Garimella, M.J. Shashkov, Untangling of 2D meshes in ALE simulations, J. Comput. Phys. 196 (2004) 627–644.
[15] A. Beskok, T.C. Warburton, Arbitrary Lagrangian Eulerian analysis of a bidirectional micro-pump using spectral elements, Int. J. Comput. Eng. Sci. 2 (1) (2001) 43–57.
[16] M.S. Gadala, Recent trends in ALE formulation and its applications in solid mechanics, Comput. Methods Appl. Mech. Eng. 193 (45–47) (2004) 4857–4873.
[17] Femlab ALE Models Reference Guide, Comsol, AB, 2004. http://www.comsol.com.
[18] M.S. Gadala, M.R. Movahhedy, J. Wang, On the mesh motion for ALE modelling of metal forming processes, Finite Elem. Anal. Des. 38 (2002) 435–459.
[19] J.O. Hallquist, Simplified arbitrary Lagrangian–Eulerian LS-DYNA Theoretical Manual, Livermore Software, 1998, Chapter 14.

## Biographies

**Isabelle P.F. Harouche** received her BSc in 1998 from the Rio de Janeiro State University in Rio de Janeiro, Brazil. She is presently pursuing her MSc in Electrical Engineering at the University of Manitoba in Winnipeg, Man., Canada. Her current research interests are the design and fabrication of MEMS devices, as well as the use of finite element analysis in MEMS simulation.

**Cyrus Shafai** is an associate professor in the Department of Electrical and Computer Engineering at the University of Manitoba. He received his BSc (Electrical Engineering) and MSc (Electrical Engineering) from the University of Manitoba, Winnipeg, Man., Canada, in 1990 and 1993, respectively. In 1997, he received the PhD degree in Electrical Engineering from the University of Alberta, Edmonton, Alta., Canada. His principle research was the development of a micromachined on-chip Peltier heat pump. His current research includes MEMS-based frequency agile antenna, phase shifters, micro-sensors.